This paper can be found at https://doi.org/10.1617/s11527-021-01706-w

Slip rate effects and cyclic behaviour of textile-to-matrix bond in textile reinforced mortar composites

Ali Dalalbashi[1]*, Stefano De Santis[2], Bahman Ghiassi[3], Daniel V. Oliveira[4]

[1] ISISE, University of Minho, Department of Civil Engineering, Guimarães, Portugal. E: alidalalbashi@gmail.com. https://orcid.org/0000-0003-0486-1433
[2] Roma Tre University, Department of Engineering. Rome, Italy. E: stefano.desantis@uniroma3.it. https://orcid.org/ 0000-0002-0816-4865
[3] University of Nottingham, Faculty of Engineering, Nottingham, United Kingdom. E: bahman.ghiassi@nottingham.ac.uk. http://orcid.org/0000-0003-4212-8961
[4] ISISE & IB-S, University of Minho, Department of Civil Engineering, Guimarães, Portugal. E: danvco@civil.uminho.pt. http://orcid.org/0000-0002-8547-3805

* Corresponding author.

ABSTRACT

The structural effectiveness of textile reinforced mortar (TRM) composites relies on their load transfer capacity to the substrate and the interaction between textile and mortar. The bond plays a crucial role in mechanism of TRM composites. Despite some recent investigations, a deep understanding still needs to be gained on the textile-to-mortar bond to develop suitable analytical and numerical predictive models, improve test methods, and orient design criteria. This work describes a laboratory study in which pull-out tests were carried out to investigate the effect of the slip rate and cyclic loading on the textile-to-mortar bond behaviour. Alkali-resistant glass fabric and sgalvanised ultra-high tensile strength steel cords embedded in two different lime-based mortars were tested. The pull-out response was sensitive to the strain rate at low rates. Cyclic loading produced a strength degradation, which reduced with the number of cycles.

Keywords

Textile reinforced mortar (TRM); Steel reinforced grout (SRG); Pull-out test; Alkali resistant glass fabrics; Cyclic behaviour; Strain rate effects.

1. INTRODUCTION

Textile reinforced mortar (TRM) composites are an emerging solution for the repair and strengthening of existing structures. They are comprised of a high-strength textile bonded with an inorganic matrix. Either bidirectional meshes of basalt, carbon, alkali-resistant glass, aramid, or PBO yarns (bundles) or unidirectional textiles of ultra-high tensile strength steel cords are used. Textiles are bonded employing matrices such as cement, lime, or geopolymer mortars. Besides TRM, other names and acronyms are used in scientific and technical documents, such as fabric reinforced cementitious matrix (FRCM), inorganic matrix-based composites, and (when comprising steel textiles) steel reinforced grout (SRG). Even though TRMs are often considered innovative strengthening systems, they have been developed more than fifteen years ago [1, 2]. Since then, several research studies have investigated their mechanical properties and the response of retrofitted structures [3].

On the one hand, experimental outcomes prove the effectiveness of TRM for enhancing the ultimate strength of reinforced concrete [4–7] and masonry [8–15] structures. With the aim of exploiting the advantages of small thickness, high strength-to-weight ratio, ease of installation in different shapes, and compatibility with many substrate materials (e.g., brick, stone, concrete), a wide range of systems have been made available in the market. As a result, TRM composites are frequently used in structural rehabilitation, especially for seismic retrofitting, applications to architectural heritage, and post-earthquake reconstruction. On the other hand, laboratory investigations show the complexity of the behaviour of TRMs, especially of the substrate-to-composite load transfer mechanisms, which determine the effectiveness of externally bonded reinforcements. The non-linear response and brittle failure of inorganic matrices entail a high sensitivity to manufacturing, installation, and curing conditions. Textile architecture and presence of coating/impregnation, mortar strength and stiffness, and roughness and porosity of the substrate also play a crucial role in the substrate-to-TRM bond. These parameters also affect the mode of failure, which may take place by cohesive debonding within the substrate, detachment between matrix and substrate or between textile and matrix, and textile slippage within the matrix [16]. TRM-to-substrate shear bond tests efficiently provide, among all the possible failure modes, the weakest one and the corresponding capacity and, therefore, are recommended for system certification [17] and for deriving TRM design parameters [18].

Many investigations have been devoted to the TRM-to-substrate bond [19–24], but only a few have explicitly focussed on the textile-to-mortar interaction . Indeed, some studies on textile-reinforced concrete (TRC) [25, 26] had already tackled this issue more than 10 years ago [27–29]. It has been studied more recently starting from the results of shear bond tests [30] or through pull-out tests with setups specifically designed to isolate the textile-to-matrix load transfer mechanism [31–33], and testing steel cords and lime mortars, which were out of TRC scopes. Experimental outcomes have shown the main parameters affecting the textile-to-mortar interaction. The layout of the textile and the roughness of its surface influence the mechanical interlocking with the mortar. The presence of coating or impregnating resins affects the chemical bond with the mortar [34]. The strength of the mortar and its curing duration [35] and conditions [36] affect the load transfer mechanism with the textile. Finally, the filaments bond in a yarn plays an important role; it is improved by the deep penetration of resin or mortar in the cross-section of the yarn, whereas when the bond between the outer filaments and the mortar is stronger than that between the outer and the inner filaments telescopic failure may occur [28]. Load-slip curves generally exhibit a first stage, during which the load transfer relies on chemical bond and interlocking, followed by a second stage associated with the onset of relative slippage and the combined contribution of adhesion and friction, and by a final stage, in which the load transfer relies on friction only [32].

Among the issues that still deserve further investigation, the effects of slip rate and the response under cyclic loading are significant to develop analytical and numerical predictive models, improve test methods, and orient design criteria. This paper describes an experimental study performed on two TRM composites, which comprised either alkali-resistant glass yarns or sgalvanised ultra-high tensile strength steel (UHTSS) cords embedded in lime-based mortars. Pull-out tests were carried out with different displacement rates to investigate the effect on the textile-to-mortar bond response and contribute to developing reliable test methods for both research and certification purposes. Then, cyclic tests were performed to detect possible deterioration of the bond capacity induced by unloading-reloading and provide a preliminary estimate of the residual bond capacity for serviceability assessment.

2. EXPERIMENTAL PROGRAMME

2.1. Materials under investigation

Two commercial hydraulic lime-based mortars, referred to as M1 and M2 throughout this paper, and two glass and steel textiles were used. Mortar M1 was a high-ductility hydraulic lime mortar [37], prepared by mixing the powder with the liquid provided by the manufacturer (5:1 powder to liquid ratio according to the technical datasheets) in a low-speed mechanical mixer for four minutes to form a homogenous paste. Mortar M2 [38] comprised a pure natural hydraulic lime (NHL 3.5) and mineral geo-binder and was prepared by mixing 1 kg powder with 0.212 kg water for seven minutes. According to the technical datasheets, the compressive elasticity modulus at 28 days are 8 GPa for M1 and 9 GPa for M2.

The glass textile was a woven biaxial mesh (25 mm × 25 mm grid spacing) made of alkali-resistant glass yarn, in which weft (longitudinal) yarns pass through the warp (transversal) yarns and are stitched to them. Its cross-sectional area per unit width was 35.27 mm^2/m [39]. The unidirectional steel textile was made of sgalvanised UHTSS micro-cords [40]. Each cord consisted of five individual wires twisted together; three straight wires wrapped by two wires at a high twist angle. The textile had a surface mass density of 670 g/m^2, a cord spacing of 6.35 mm, and a cross-sectional area per unit width of 84 mm^2/m.

2.2. Material scharacterisation tests

Compressive and flexural strength tests were performed on mortars at the age of 60 days, according to relevant standards (ASTM C109 [41] and EN 1015-11 [42]). Five cubics (50×50×50 mm^3) specimens were prepared for the compressive tests and five prismatic (40×40×160 mm^3) specimens for the bending tests. The tests were carried out with a Lloyd testing machine under force control at rates of 150 N/s (for compressive tests) and 10 N/s (for bending tests). In the compressive tests, a pair of Teflon sheets with a layer of oil in between was placed between the loaded surfaces of the specimen and the compression plates to reduce friction. Bending tests were performed according to the three-point bending test scheme with a 100 mm distance between the supports. The experimental results showed an average compressive strength of 8.36 MPa (coefficient of variation: CoV= 15 %) and average flexural strength of 4.49 MPa (CoV= 9 %) for mortar M1, whereas these values were 7.47 MPa (CoV= 5 %) and 1.78 MPa (CoV= 10 %), respectively, for mortar M2.

The tensile response of the textiles was characterised by performing direct tensile tests on single yarn/cord using a universal testing machine with a maximum load capacity of 10 kN, based on [21, 22]. These tests were performed under displacement control at a rate of 0.3 mm/min. Five specimens with a free length of 300 mm were tested for each textile. A 100 mm clip gauge was located at the centre of the specimens to measure the strain. The average tensile stress, Young's modulus (E_f), and ultimate strain (axial strain at peak stress) were obtained as 875 MPa (CoV= 13 %), 65.9 GPa (CoV= 5 %), and 0.0177 mm/mm (CoV= 10 %) for the glass yarns, and 2972 MPa (CoV= 8 %), 189.3 GPa (CoV= 8 %), and 0.0188 mm/mm (CoV= 9 %) for the steel cords.

2.3. Pull-out tests

2.3.1. Geometry and manufacturing of specimens

The textile-to-mortar bond behaviour was investigated using a single-sided pull-out test setup developed and presented in [32]. To manufacture the specimens, a 200 mm textile was first embedded in an epoxy resin block, as shown in Fig. 1a, b.The opposite end of the textile was then embedded in a tile-shaped mortar block with a cross-section of 125 × 16 mm^2 (Fig. 1c). For detailed information on the procedure followed for preparing the specimens, the reader is referred to [32]. The specimens were demolded after three days of casting, were cured in a damp environment for seven days, and then stored in laboratory environmental conditions (20°C, 60% RH) for 50 days. The final age of the specimens at testing was 60 days.

2.3.2. Test setup

The pull-out tests were performed using either a servo-hydraulic system with a load capacity of 25 kN (for monotonic tests) or a universal testing machine with a load capacity of 10 kN (for cyclic tests). This change of the testing system was due to the unavailability of the servo-hydraulic system when cyclic tests were performed. All the tests were performed under displacement control, and the machine stroke displacement was controlled.

The mortar blocks were fixed by U-shaped steel support to a rigid frame, integral with the lower crosshead of the testing machine, whereas a mechanical clamp gripped the unbonded yarn/cord embedded in the epoxy resin from the top (Fig. 1d). Two LVDTs with a 20 mm range and 2-μm sensitivity were placed at the two sides of the epoxy block to record the relative displacement between the mortar and the textile at the loaded end of the bonded length (upper surface of the mortar block). The slip (showed hereinafter in the paper) was calculated as the average of the two displacements measured by these LVDTs.

2.3.3. Monotonic test protocol

To investigate the slip rate effect on the textile-to-matrix bond behaviour, monotonic tests were performed on specimens comprising a single glass yarn, extracted from the textile mesh in the longitudinal (warp) direction or a single steel cord. Mortar M1 was used to manufacture all the specimens for these tests. The bond lengths (L_b) were 50 mm for the glass yarns and 150 mm for the steel cords, equal to the effective bond lengths, as determined in [34]. The effective bond length was defined as the embedded length in which the load corresponding to the complete debonding did not change at the load-slip curve (bond leghts longer than the effective bond length do not entail any increases of the debonding load). Five different slip rates were considered, namely 0.2, 1.0, 5.0, 10.0, and 20.0 mm/min. Five specimens were prepared and tested for each slip rate, resulting in 25 specimens for the glass TRM and 25 for the steel TRM (Table 1).

2.3.4. Cyclic test protocol

Cyclic pull-out tests were performed on glass yarns and steel cords embedded in M1 and M2 mortar matrices. Loading-unloading cycles were performed with progressively increasing maximum (target) slip, from 0.3 mm to 20 mm, whereas the minimum slip was that corresponding a load of 50 N in the unloading phase, to avoid yarn/cord instability and ensure that its position was kept. Two cycles for each target slip were carried out, with a slip rate of 1.0 mm/min (up to a target slip of 9 mm) and of 3.0 mm/min (increased for a timesaving reason) until the end of the tests (Fig. 1e).

In cyclic tests, various configurations were considered, as shown in Fig. 1a, b . More specifically, in some of glass TRM specimens, the yarn was not provided with transverse (weft) elements (the orthogonal yarns were cut before casting, as in monotonic tests) and L_b was either 50 mm or 75 mm, whereas in other specimens transverse elements were left embedded in the mortar, and L_b was 50 mm (Fig. 1a). The transverse elements had a total length of 25 mm, 12.5 mm at each side, equal to half of the mesh size. Furthermore, some specimens comprised two fibre yarns and were provided with two transverse elements, with L_b= 50 mm or L_b= 75 mm (Fig. 1a). All specimens of glass TRM were manufactured with M1 mortar. As concerns steel TRM, the parameters investigated were mortar type (the two mortars, M1 and M2, were used), L_b (50 mm and 150 mm), and the number of steel cords (in addition to one cord, two cords in M1 and M2, and four cords in M1, always with L_b= 150 mm), as presented in Fig. 1b. Note that the steel textile is unidirectional, and there are no weft elements.

3. SLIP RATE EFFECT

3.1. Reliability and physical meaning of test outcomes

As explained before, the specimens prepared for pull-out tests consisted of a free yarn/cord length, which was embedded in an epoxy block resin to facilitate gripping of the samples by the wedges of the testing machine. Nevertheless, as the tests were performed by imposing displacement rates to the hydraulic system, it was necessary to check the actual slip rates at the loaded end of the bonded area (upper surface of the mortar block), measured by the LVDTs.

Fig. 2 showed the changes in the actual slip rate versus slip for the different imposed (machine stroke) slip rates. The actual slip rate was computed by dividing the textile slip (measured by the LVDTs) into the experimental time. For better understanding, these changes were presented in the complete and enlarged scales for both the glass and steel-based TRM composites in Fig. 2a and Fig. 2b, respectively. For both systems, the slip rate reached the expected value in the early stages of the tests, namely, at about 0.03 mm in the specimens tested at 0.2 mm/min and 1.0 mm/min rates, and about 0.4 mm for those tested at higher slip rates. In glass TRMs tested at 0.2 mm/min and 1.0 mm/min rates and in all steel TRMs, these slip values were lower than the slip corresponding to the first peak load, S_{p1}, so the bond behaviour was still in the elastic stage, and no delamination has occurred. On the other hand, in glass TRMs tested with a slip rate equal or higher than 5 mm/min, these slip values were larger than S_{p1}, indicating the tests reached the intended slip rate after debonding had initiated. These comparisons validate the experimental setup developed for the tests presented in this study and the slip rate selected for the first part of the cyclic tests. At the same time, they indicated the need to represent the results in terms of actually measured slip and actual slip rate (e.g., at peak load), instead of controlled machine stroke displacement and imposed sip rate, also in order to make test outcomes independent from test implementation details.

3.2. Glass TRM specimens

The typical load versus slip response curve of a monotonic pull-out test is shown in Fig. 1f. In the first static ascending branch, which includes an initial linear elastic phase and a non-linear pre-peak phase, the load transfer between textile and mortar relies on adhesion (debonding phase). When a peak load (P_{P1}) is attained, the complete debonding occurs, and the dynamic stage initiates, in which the load transfer mechanism relies only on friction [43–46]. For further information about the pull-out mechanism of TRM composites, the reader is reffered to [32].

The transition between static and dynamic ranges can either be a sudden drop in the pull-out force if the frictional bond is smaller than the adhesive bond (the load suddenly drops down to a residual value P_F, which shares the same slip with P_{P1}, which is named as S_F) or can be smooth [44, 45, 47, 48]. In the dynamic stage, either a slip hardening or a slip softening effect can be observed [45]. When a slip hardening is observed in the dynamic stage, the load increases with a lower slope than that of the static one. A recent study attributes this slip hardening to the damage of the surface of the fibre yarn, which is due to its interaction with the matrix as a result of pull-out activation [34, 43, 45, 46, 49–51], but further investigations are still needed to understand better the mechanisms behind this observation. As the test progresses, the portion of the textile-to-mortar interface where friction holds progressively becomes smaller as the debonding length becomes larger. A second load peak (P_{P2}) is attained (at a slip of S_{P2}) when the interaction of the damaged yarn surface is diminished, and friction becomes the sole resistance mechanism. With the increment of the debonded length, the load resistance of the system reduces until the end of the tests.

The curves obtained from the experiments on glass TRM composites are shown in Fig. 3, in which each subplot from (a) to (e) collects the curves, detected under the same slip rate, of the individual tests and the average one, whereas subplot (f) shows the five average curves together to compare the different slip rates. The average load values P_{P1}, $P_{F,}$ and P_{P2} are compared in Fig. 4a. The mean debonding peak loads (P_{P1}) vary between 153 N (at 0.2 mm/min slip rate) and 340 N (at 10 mm/min), whereas the second peak loads range between 144 N (0.2 mm/min) to 386 N (at 10 mm/min), as listed in Table 2. It is worth noting that these peaks are of the same order of magnitude and that the former is not necessarily higher than the latter.

Pull-out tests revealed that the bond behaviour in terms of peak load was affected by the slip rate. More specifically, for low rates when passing from 0.2 mm/min to 1.0 mm/min and to 5 mm/min, the higher was the slip rate, the higher were P_{P1} and P_{P2}. In contrast, a quasi-sstabilisation was found for the higher rates

(5 mm/min, 10 mm/min, and 20 mm/min). On the other hand, the load drop amount after full debonding ($P_{P1} - P_F$) seems to be independent of the load rate.

A similar trend was also found on the pull-out energy (E_{po}, see also Fig. 1f) as shown in Fig. 4b, and on the chemical bond energy (G_d, Table 2), defined by Eq. 1, in which E_f is the modulus of elasticity of the glass textile and d_f is the diameter of the yarn (1.06 mm) [43, 44, 46].

$$\left\{ G_d = \frac{2\left(P_{P1} - P_F\right)^2}{\pi^2 E_f d_f^3} \right\} \quad (1)$$

The debonding energy (E_{deb}), calculated as the area below the response curve until P_{P1} (Fig. 1f), was smaller than the pull-out energy, and its changes with the increment of the slip rate were less significant. The initial axial stiffness (K, as defined in Fig. 1f) showed a large scatter but still following a similar trend as the load peaks, as illustrated in Fig. 4c. By contrast, the values obtained under the slowest rates were always lower than the other ones, confirming that very slow tests may provide lower results. Finally, no clear effect of the slip rate was observed on the slip values, S_{P1}, S_F, and S_{P2} (Table 2).

In summary, based on the results of the pull-out tests performed on the glass TRM system investigated in this work, and limited to the experimental setup used and the slip rate range considered, the influence of the slip rate was negligible between 5 mm/min and 20 mm/min. In contrast, it led to a reduction of the bond strength for lower rates (below 5 mm/min).

3.3. Steel TRM specimens

Fig. 5 shows the load versus slip response curves of the monotonic pull-out tests on steel TRM systems. As for the glass TRM ones, subplots (a-e) refer to homogeneous slip rates, and subplot (f) collects the five average curves. The first stage of the test was associated with a stiff branch of the response curves, in which the load transfer between cord and matrix relied on both adhesion and interlocking, this latter arising by the high roughness of the cord surface. Then, the curves displayed a progressive reduction of the slope, up to the attainment of the load peak, followed by a post-peak softening phase with a nearly linear load reduction associated with the increase of slip. The transition between first and second stages was much smoother than in glass TRM, there were no sudden load drops associated with brittle failures, such that, in this case, a precise value of the loads corresponding to the loss of adhesion and its residual value after the load drop could not be identified. For this reason, Fig. 6a and Table 2 do not include P_{P2}, P_F, nor S_{P2}, S_F, and G_d, which could not be determined.

The maximum load (P_{P1}), resulting from the contributions of adhesion, interlocking and friction, increased from 328 N (at 0.2 mm/min slip rate) to 507 N (20 mm/min), without a clear trend with the increase of slip rate (Fig. 6a). The strength at the slowest rate (0.2 mm/min), however, confirmed itself as the lowest one. Noteworthy is that, for each slip rate, the peak load attained by steel TRM was higher than the corresponding value recorded in the tests on glass TRM, by virtue of the higher contribution provided by friction and adhesion, which, in its turn, was due to the better adhesion of cords with the mortar as well as the roughness of the cord surface and the more effective load transfer capacity provided by interlocking and friction. As for the glass

TRMs, also in the steel TRM composites the pull-out behaviour was affected by the slip rate at the lowest rates considered in this investigation. The bond capacity at 0.2 mm/min resulted lower than those obtained at all the other rates. On the other hand, the differences amongst such higher rates (from 1 mm/m in to 20 mm/ min, Table 2) were of the same order of magnitude of the scatter, so no clear trends emerged.

The debonding energy (E_{deb}) in steel TRM system was, in general, significantly higher than that of glass TRM, whereas the pull-out energies (E_{po}) were comparable (Fig. 6b). Both debonding and pull-out energies showed slight variations with the slip rate beyond 0.2 mm/min. The slip S_{P1} also appeared independent from the slip rate (Table 2). Finally, the initial stiffness (K), decreased until a slip rate of 5 mm/min and then it did not change, showing an opposite trend compared to the glass TRM system. This output should be further investigated considering also other types of steel cords.

4. CYCLIC BEHAVIOUR

4.1. Glass TRM specimens

The experimental results of cyclic pull-out tests on glass TRM composites are shown in Fig. 7-Fig. 9. Subplots (a) display the load versus slip response curves. Subplots (b) show the peak loads attained in each cycle, and are represented at the corresponding target slip, as shown in Fig. 1g. More specifically, the first two peaks (Peak-1 and Peak-2) were followed by an unloading phase, whereas the third one (Peak-3) was attained during a longer loading phase, which ended at the following target slip (see the cyclic test protocol in Fig. 1e). In subplots (a) and (b) the load is referred to the single yarn to allow comparisons between specimens with one yarn and those with groups of yarns. Subplots (c) show the strength degradation, calculated (in percent) at each cycle (i.e., at each target slip) as the reduction of Peak-2 with respect to Peak-1 (Cycle-1) and that of Peak-3 with respect to Peak-2 (Cycle-2), see Fig. 1g. Finally, subplots (d) represent the reduction of stiffness detected in cycles 2 and 3, with respect to that of the previous cycle, the stiffness corresponding to the secant modulus of elasticity of the loading branch between its first point and the target slip (Fig. 1g), as follows:

$$\begin{cases} \Delta K_1 = \left(1 - \dfrac{K_1^i}{K_{1,max}}\right) \times 100 \\ \Delta K_2 = \left(1 - \dfrac{K_2^i}{K_{2,max}}\right) \times 100 \end{cases} \tag{2}$$

Where K_1^i, and $K_{1,\,max}$ were the slop of the first load cycle at the slip "i", and the slop corresponding to the maximum stiffness of the same test group, respectively. The same function was employed for the second cycle.

Some common features emerged in all specimens, independently from their specific configuration. First, un-loading-reloading cycles were very narrow, indicating a small amount of dissipated energy, and the cyclic test results contained in the envelope of the monotonic one. Second, under repeated cycles at the same target slip, the peak load at the end of the first loading phase was not recovered after the cycles, i.e., a strength degradation resulted due to the irreversible loss of adhesion, especially in the first cycle. More precisely, the strength degradation after the first cycle, represented by the difference between Peak-1 and Peak-2 in subplots

(b) and by the curve of Cycle-1 in subplots (c), was comprised between 15 % and 45 %. The peak loads after two cycles (Peak-3), instead, were similar to those after one cycle (Peak-2); the strength degradation curve of Cycle-2 was lower than that of Cycle-1, and comprised between 5 % and 25 %. On the other hand, for both Cycle-1 and Cycle-2, no clear correlation resulted between strength degradation and slip. Finally, the stiffness degradation varied in the 5- 15 % range at small slips (less than 1 mm), increased up to 50- 75 % at 15 mm slip, and was similar in Cycle-1 and in Cycle-2, as shown in subplots (d).

There were also some differences amongst the different configurations investigated. First, a higher maximum load was attained by the specimens with the single yarn with L_b= 75 mm (Fig. 7a, b) with respect to L_b= 50 mm (Fig. 7a, b and Fig. 8a, b), indicating that a longer bond length led to a higher pull-out strength, which, in its turn, may be due either to an effective bond length longer than 50 mm or to a higher contribution of friction activated over a longer embedded yarn (or to a combination of the two factors). At the same time, L_b= 75 mm showed a smaller strain (slip) capacity when compared to L_b= 50 mm (around 1/3) that is due to the early occurrence of the yarn rupture. These observations are also in line with the ones previously reported on monotonic response of the same glass TRM system tested under different embedded lengths [34]. Also, the single yarn with L_b= 75 mm showed a smaller load degradation of Cycle-1 and Cycle-2 while similar stiffness degradation compared to L_b= 50 mm.

The role of transverse yarns on the cyclic response was also significant (Fig. 8). A clearly larger Peak-1, Peak-2 and Peak-3 was obtained in the specimens with transverse yarns when compared to those with a single longitudinal yarn. At the same time, single yarns showed a larger strength degradation in both Cycle-1 and Cycle-2. A higher pull-out load/yarn was also obtained with two fibre yarns (Fig. 9a, b) with respect to one yarn (note that, as said before, the load is always indicated per yarn, i.e., the force recorded by the load cell was divided by the number of yarns to plot the results). This again shows the beneficial role of interaction between fibre yarns connected by weft elements, as also previously reported in [34].

4.2. Steel TRM specimens

Fig. 10 to Fig. 13 show the cyclic response of steel TRM composites, namely, load versus slip response curves in subplots (a), peak loads at target slips (b), strength degradation (c), and stiffness degradation (d). As in glass TRMs, the cyclic curves displayed narrow cycles with small energy dissipated by hysteresis. Moreover, the monotonic curves could be considered as envelopes of the cyclic ones. Cyclic loading led to a strength degradation, which was higher after the first cycle (10- 35 %) than after the second cycle (5- 20 %, with only few exceptions), suggesting that a residual bond strength could be attained with few more cycles. The stiffness degradation in the two cycles was comparable and comprised between 10- 30% at small slips (below 3 mm) and 50- 75 % at the end of the test (15 mm slip).

The comparisons amongst different configurations showed the role of embedded length and type of mortar, confirming the outcomes of previous monotonic studies [33–35]. The maximum load attained by a single cord in M2 mortar with L_b= 50 mm (246.5 N, Fig. 10b) was much lower than that exhibited with mortar M1 (519.1 N, Fig. 10b), clearly showing the role of mortar properties on the bond performance. Mortar M1, despite a similar compressive strength and elastic modulus, showed a larger flexural strength compared to mortar M2.

The better flexural tensile strength of this mortar, which can be due to the presence of short fibres in the mix and differences in the chemistry of these mortars, appeared as a good indicator for the bond performance with the textile. Also, the enhancement of the bond response when the embedded length is increased from 50 mm to 150 mm was different. In contrast to the specimens with mortar M2, the bond behaviour did not show a significant improvement when the embedded length was increased in specimens with mortar M1, which could be attributed to the differences in the effective embedded length in these two systems.

The UHTSS textile being unidirectional, the effect of the number of cords was expected to be insignificant. Nevertheless, the peak loads per cord with M1 mortar were 611.9 N with 1 cord (Fig. 11b), 783.6 N with 2 cords (Fig. 12b) and 983.8 N with 4 cords (Fig. 13b), showing an increase in the load bearing capacity by each cord when the number of cords increases. In contrast, in samples with M2, the peak load difference is insignificant (819 N with 1 cord (Fig. 11b) and 907 N with 2 cords (Fig. 12b), (in all cases L_b was 150 mm). Indeed, the interaction between cords was much weaker due to the absence of weft (transversal) elements with respect to that experienced by bidirectional meshes and, therefore, the beneficial effects observed with the groups of glass yarns (discussed in the previous section) were much less pronounced in this case. Finally, and as in glass TRMs, also for steel ones the energy absorption levels were smaller in cyclic tests with respect to of monotonic tests.

5. CONCLUSIONS

Displacement controlled pull-out tests were carried out under monotonic and cyclic loading to investigate the textile-to-matrix load transfer mechanism in glass and steel TRM composites. The experimental setup was designed to control the rate of the relative displacement (slip) between yarn (or cord) and matrix at the first bonded section. The bond behaviour was scharacterised by a first stage, in which the load transfer relied on adhesion, followed by a second stage in which friction also significantly contributed after the onset of a relative slippage of the textile within the matrix. A contribution of interlocking was also detected in steel TRM composites, due to the rough surface of steel cords.

The bond strength was affected by the slip rate at low rates (it was lower below 1 mm/min than beyond this threshold), whereas no significant variation of peak loads was detected in faster tests (up to 20 mm/min). Despite the scatter of test outcomes (due to the brittle nature of the mortar matrices and of the adhesion phenomena investigated), similar trends were observed also for absorbed energy and stiffness, confirming the sensitivity to the slip rate in slow tests. Clearly, other TRM materials may exhibit different sensitivity and it the results obtained in this investigation are hardly extendable to composites with different fabrics and mortars, as well as to different manufacturing and curing conditions. It was also observed that in the glass TRMs the intended slip rate was reached only after the peak load in samples tested under high slip rates.

The cyclic response was scharacterised by narrow unloading-reloading cycles, indicating a small amount of hysteretic energy dissipation. The cyclic curve was contained in the envelope of the monotonic one. Cyclic loading led to a pull-out strength degradation, especially after the first cycle and in the order of 25-35%. Its reduction with the increase of performed cycles indicated that a residual strength can eventually be identified.

The stiffness degradation, instead, varied in the 5-15% range at small slips (less than 1 mm), and increased up to 50-75% at 15 mm slip for both the first and the second load cycled performed in the tests. The bidirectional glass mesh exhibited an effective interaction between fibre yarns, which was much less pronounced in the cords of the uniaxial UHTSS textile, which is not provided with weft (transversal elements).

Future investigations can be oriented by the experimental results obtained in this study to develop a deeper understanding on the textile-to-matrix bond behaviour, with an impact on testing protocols and design relationships. As for the former, the knowledge of the sensitivity to slip rate is useful to integrate the outcomes of previous studies [32, 34] and support comparisons between different investigations. As for the latter, the execution of cyclic tests can provide the residual bond strength under unloading-loading cycles, which may be considered as lower bound threshold and associated with permissibility limit state conditions.

ACKNOWLEDGEMENTS

Kerakoll SpA (Sassuolo, MO, Italy) is kindly acknowledged for supplying reinforcement materials. Additionally, the authors wish also to thank Andrea Della Torre (master student) who helped with the experimental part.

COMPLIANCE WITH ETHICAL STANDARDS

This work was partly financed by FEDER funds through the Competitivity Factors Operational Programme (COMPETE) and by national funds through the Foundation for Science and Technology (FCT) within the scope of the project POCI-01-0145-FEDER-007633. The first author has received grant from the Foundation for Science and Technology (FCT), with grant number: SFRH/BD/131282/2017. The second author acknowledges funding by Regione Lazio within the Research Project "SiCura, Sustainable technologies for the seismic protection of the cultural heritage" (2018-2020, N. 15136), by the Italian Civil Protection Department within the Research Project "ReLUIS" (2019-2021) and by the Italian Ministry of Education, University and Research (MIUR), in the frame of the Departments of Excellence Initiative (2018-2022), attributed to the Department of Engineering of Roma Tre University.

REFERENCES

1. Barton B, Wobbe E, Dharani LR, et al (2005) Characterization of reinforced concrete beams strengthened by steel reinforced polymer and grout (SRP and SRG) composites. Mater Sci Eng A 412:129–136. https://doi.org/10.1016/j.msea.2005.08.151
2. Triantafillou TC, Papanicolaou CG (2005) Textile reinforced mortars (TRM) versus fiber reinforced polymers (FRP) as strengthening materials of concrete structures. In: the 7th International Symposium on Fiber- Reinforced (FRP) Polymer Reinforcement for Concrete Structures (FRPRCS-7): ACI SP-230-6. pp 99–118
3. Ghiassi B (2019) Mechanics and durability of textile reinforced mortars: a review of recent advances and open issues. RILEM Tech Lett 4:130–137. https://doi.org/10.21809/rilemtechlett.2019.99
4. Loreto G, Babaeidarabad S, Leardini L, Nanni A (2015) RC beams shear-strengthened with fabric-reinforced-cementitious-matrix (FRCM) composite. Int J Adv Struct Eng 7:341–352. https://doi.org/10.1007/s40091-015-0102-9
5. Napoli A, Realfonzo R (2015) Reinforced concrete beams strengthened with SRP/SRG systems: Experimental investigation. Constr Build Mater 93:654–677. https://doi.org/10.1016/j.conbuildmat.2015.06.027
6. Pino V, Akbari Hadad H, De Caso y Basalo F, et al (2017) Performance of FRCM-Strengthened RC Beams Subject to Fatigue. J Bridg Eng 22:. https://doi.org/10.1061/(ASCE)BE.1943-5592.0001107
7. Raoof SM, Koutas LN, Bournas DA (2017) Textile-reinforced mortar (TRM) versus fibre-reinforced polymers (FRP) in flexural strengthening of RC beams. Constr Build Mater 151:279–291. https://doi.org/10.1016/j.conbuildmat.2017.05.023

8. Borri A, Casadei P, Castori G, Hammond J (2009) Strengthening of brick masonry arches with externally bonded steel reinforced composites. J Compos Constr 13:468–475. https://doi.org/10.1061/(ASCE)CC.1943-5614.0000030
9. Papanicolaou C, Triantafillou T, Lekka M (2011) Externally bonded grids as strengthening and seismic retrofitting materials of masonry panels. Constr Build Mater 25:504–514. https://doi.org/10.1016/j.conbuildmat.2010.07.018
10. Babaeidarabad S, De Caso F, Nanni A (2014) Out-of-plane behavior of URM walls strengthened with Fabric-Reinforced Cementitious Matrix Composite. J Compos Constr 549:. https://doi.org/10.1061/(ASCE)CC .1943-5614.0000457
11. Marcari G, Basili M, Vestroni F (2017) Experimental investigation of tuff masonry panels reinforced with surface bonded basalt textile-reinforced mortar. Compos Part B Eng 108:131–142. https://doi.org/10.1016/j.compositesb.2016.09.094
12. Bellini A, Incerti A, Bovo M, Mazzotti C (2018) Effectiveness of FRCM reinforcement applied to masonry walls subject to axial force and out-of-plane loads evaluated by experimental and numerical studies. Int J Archit Herit 12:. https://doi.org/10.1080/15583058.2017.1323246
13. De Santis S, Roscini F, de Felice G (2018) Full-scale tests on masonry vaults strengthened with Steel Reinforced Grout. Compos Part B Eng 141:20–36. https://doi.org/10.1016/j.compositesb.2017.12.023
14. De Santis S, De Canio G, de Felice G, et al (2019) Out-of-plane seismic retrofitting of masonry walls with textile reinforced mortar composites. Bull Earthq Eng 17:6265–6300. https://doi.org/10.1007/s10518-019-00701-5
15. De Santis S, de Felice G, Roscini F (2019) Retrofitting of masonry vaults by basalt textile-reinforced mortar overlays. Int J Archit Herit 13:1061–1077. https://doi.org/10.1080/15583058.2019.1597947
16. de Felice G, De Santis S, Garmendia L, et al (2014) Mortar-based systems for externally bonded strengthening of masonry. Mater Struct 47:2021–2037. https://doi.org/10.1617/s11527-014-0360-1
17. De Santis S, Hadad HA, De Caso y Basalo F, et al (2018) Acceptance criteria for tensile characterization of fabric-reinforced cementitious matrix systems for concrete and masonry repair. J Compos Constr 22:04018048. https://doi.org/10.1061/(ASCE)CC.1943-5614.0000886
18. Meriggi P, de Felice G, De Santis S (2020) Design of the out-of-plane strengthening of masonry walls with textile reinforced mortar composites. Constr Build Mater 240:. https://doi.org/10.1016/j.conbuildmat.2019.117946
19. D'Ambrisi A, Feo L, Focacci F (2013) Experimental and analytical investigation on bond between Carbon-FRCM materials and masonry. Compos Part B Eng 46:15–20. https://doi.org/10.1016/j.compositesb.2012.10.018
20. Sneed LH, D'Antino T, Carloni C (2014) Investigation of bond behavior of polyparaphenylene benzobisoxazole fiber-reinforced cementitious matrix composite-concrete interface. ACI Mater J 111:. https://doi.org/10.14359/51686604
21. Razavizadeh A, Ghiassi B, Oliveira D V. (2014) Bond behavior of SRG-strengthened masonry units: Testing and numerical modeling. Constr Build Mater 64:387–397. https://doi.org/10.1016/j.conbuildmat.2014.04.070
22. Carozzi FG, Poggi C (2015) Mechanical properties and debonding strength of Fabric Reinforced Cementitious Matrix (FRCM) systems for masonry strengthening. Compos Part B Eng 70:215–230. https://doi.org/10.1016/j.compositesb.2014.10.056
23. De Santis S (2017) Bond behaviour of Steel Reinforced Grout for the extrados strengthening of masonry vaults. Constr Build Mater 150:367–382. https://doi.org/10.1016/j.conbuildmat.2017.06.010
24. de Felice G, D'Antino T, De Santis S, et al (2020) Lessons learned on the tensile and bond behaviour of Fabric Reinforced Cementitious Matrix (FRCM) composites. Front Built Environ 6:1–15. https://doi.org/10.3389/fbuil.2020.00005
25. Brameshuber W (2006) RILEM TC 201-TRC: Textile reinforced concrete- state-of-the-art. RILEM, Bagneux
26. Mobasher B (2012) Mechanics of Fiber and Textile Reinforced Cement Composites. Taylor & Francis Group, London- New York
27. Häußler-Combe U, Hartig J (2007) Bond and failure mechanisms of textile reinforced concrete (TRC) under uniaxial tensile loading. Cem Concr Compos 29:279–289. https://doi.org/10.1016/j.cemconcomp.2006.12.012
28. Hegger J, Will N, Bruckermann O, Voss S (2006) Load-bearing behaviour and simulation of textile reinforced concrete. Mater Struct 39:765–776. https://doi.org/10.1617/s11527-005-9039-y
29. Banholzer B (2006) Bond of a strand in a cementitious matrix. Mater Struct 39:1015–1028. https://doi.org/10.1617/s11527-006-9115-y
30. D'Antino T, Pellegrino C, Carloni C, et al (2014) Experimental Analysis of the Bond Behavior of Glass, Carbon, and Steel FRCM Composites. Key Eng Mater 624:371–378. https://doi.org/10.4028/www.scientific.net/KEM.624.371
31. D'Antino T, Carrozzi FG, Colombi P, Poggi C (2017) A New Pull-Out Test to Study the Bond Behavior of Fiber Reinforced Cementitious Composites. Key Eng Mater 747:258–265. https://doi.org/10.4028/www.scientific.net/KEM.747.258
32. Dalalbashi A, Ghiassi B, Oliveira DV, Freitas A (2018) Effect of test setup on the fiber-to-mortar pull-out response in TRM composites: experimental and analytical modeling. Compos Part B Eng 143:250–268. https://doi.org/10.1016/j.compositesb.2018.02.010
33. Ghiassi B, Oliveira D V, Marques V, et al (2016) Multi-level characterization of steel reinforced mortars for strengthening of masonry structures. Mater Des 110:903–913. https://doi.org/10.1016/j.matdes.2016.08.034

34. Dalalbashi A, Ghiassi B, Oliveira DV, Freitas A (2018) Fiber-to-mortar bond behavior in TRM composites: effect of embedded length and fiber configuration. Compos Part B Eng 152:43–57. https://doi.org/10.1016/j.compositesb.2018.06.014
35. Dalalbashi A, Ghiassi B, Oliveira D V. (2019) Textile-to-mortar bond behaviour in lime-based textile reinforced mortars. Constr Build Mater 227:116682. https://doi.org/10.1016/j.conbuildmat.2019.116682
36. Le HV, Moon D, Kim DJ (2018) Effects of ageing and storage conditions on the interfacial bond strength of steel fibers in mortars. Constr Build Mater 170:129–141. https://doi.org/10.1016/j.conbuildmat.2018.03.064
37. (2012) Planitop HDM Restauro- 1071-2-2012. In: MAPEI. https://www.mapei.com/it/en/products-and-solutions/products/detail/planitop-hdm
38. (2016) GeoCalce Fino. In: Kerakoll. https://shop.vittoriosabato.it/uploads/products/attachments/561_KERAKOLL BIOCALCE FINO KG25.pdf
39. (2019) Mapegride G220- 1033-7-2019 (GB). In: MAPEI. https://www.mapei.com/it/en/products-and-solutions/products/detail/mapegrid-g-220
40. (2014) GeoSteel G600 Code: E865 2014/07. In: Kerakoll. https://products.kerakoll.com/en/p/geosteel-g600
41. (2005) ASTM C109/C109M-05, Standard test method for compressive strength of hydraulic cement mortars (Using 2-in. or [50-mm] Cube Specimens)
42. (1999) BS EN 1015-11, Methods of test for mortar for masonry. Determination of flexural and compressive strength of hardened mortar
43. Redon C, Li VC, Wu C, et al (2001) Measuring and modifying interface properties of PVA fibers in ECC matrix. J Mater Civ Eng 13:399–406. https://doi.org/10.1061/(ASCE)0899-1561(2001)13:6(399)
44. Lin Z, Kanda T, Li VC (1999) On interface property characterization and performance of fiber reinforced cementitious composites. J Concr Sci Eng RILEM 1:173–184
45. Naik DL, Sharma A, Chada RR, et al (2019) Modified pullout test for indirect characterization of natural fiber and cementitious matrix interface properties. Constr Build Mater 208:381–393. https://doi.org/10.1016/j.conbuildmat.2019.03.021
46. Boshoff WP, Mechtcherine V, van Zijl GPAG (2009) Characterising the time-dependant behaviour on the single fibre level of SHCC: Part 2: The rate effects on fibre pull-out tests. Cem Concr Res 39:787–797. https://doi.org/10.1016/j.cemconres.2009.06.006
47. Li VC, Wu HC, Chan YW (1995) Interfacial property tailoring for pseudo strain- hardening cementitious composites. Adv Technol Des Fabr Compos Mater Struct Eng Appl Fract Mech 14:261–268. https://doi.org/10.1007/978-94-015-8563-7_18
48. Li VC, Wu H-C, Chan Y-W (1996) Effect of plasma treatment of polyethylene fibers on interface and ementitious composite properties. J Am Ceram Soc 79:700–704. https://doi.org/10.1111/j.1151-2916.1996.tb07932.x
49. Lin Z, Li VC (1997) Crack bridging in fiber reinforced cementitious composites with slip-hardening interfaces. J Mech Phys Solids 45:763–787. https://doi.org/10.1016/S0022-5096(96)00095-6
50. Wang Y, Li VC, Backer S (1988) Analysis of synthetic fiber pull-out from a cement matrix. Mater Res Soc Symp Bond Cem Compos 114:159–166. https://doi.org/10.1557/PROC-114-159
51. Wang Y, Lf VC, Backer S (1988) Modelling of fibre pull-out from a cement matrix. Int J Cem Compos 10:143–149. https://doi.org/10.1016/0262-5075(88)90002-4

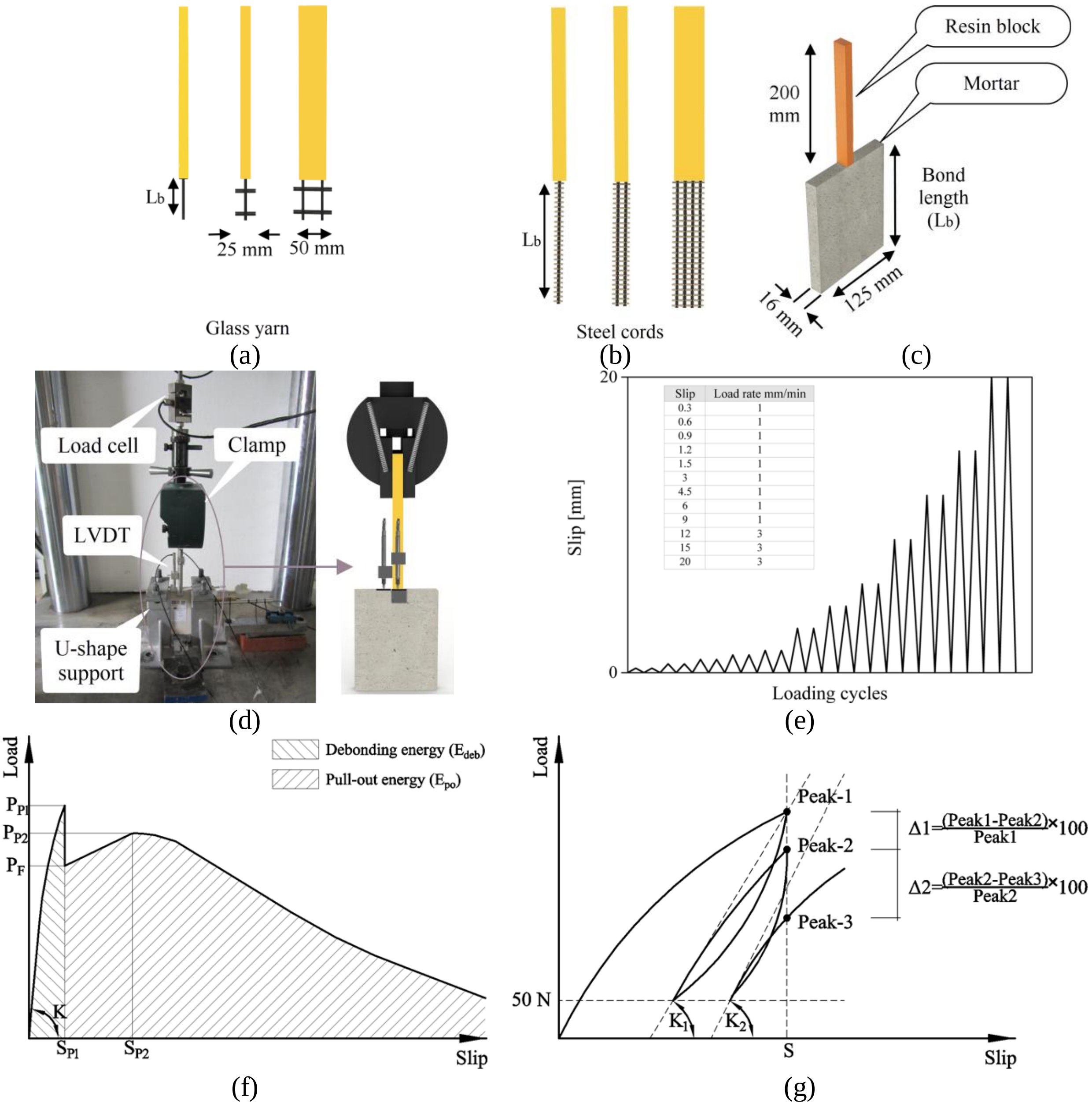

Fig. 1. Pull-out test setup.

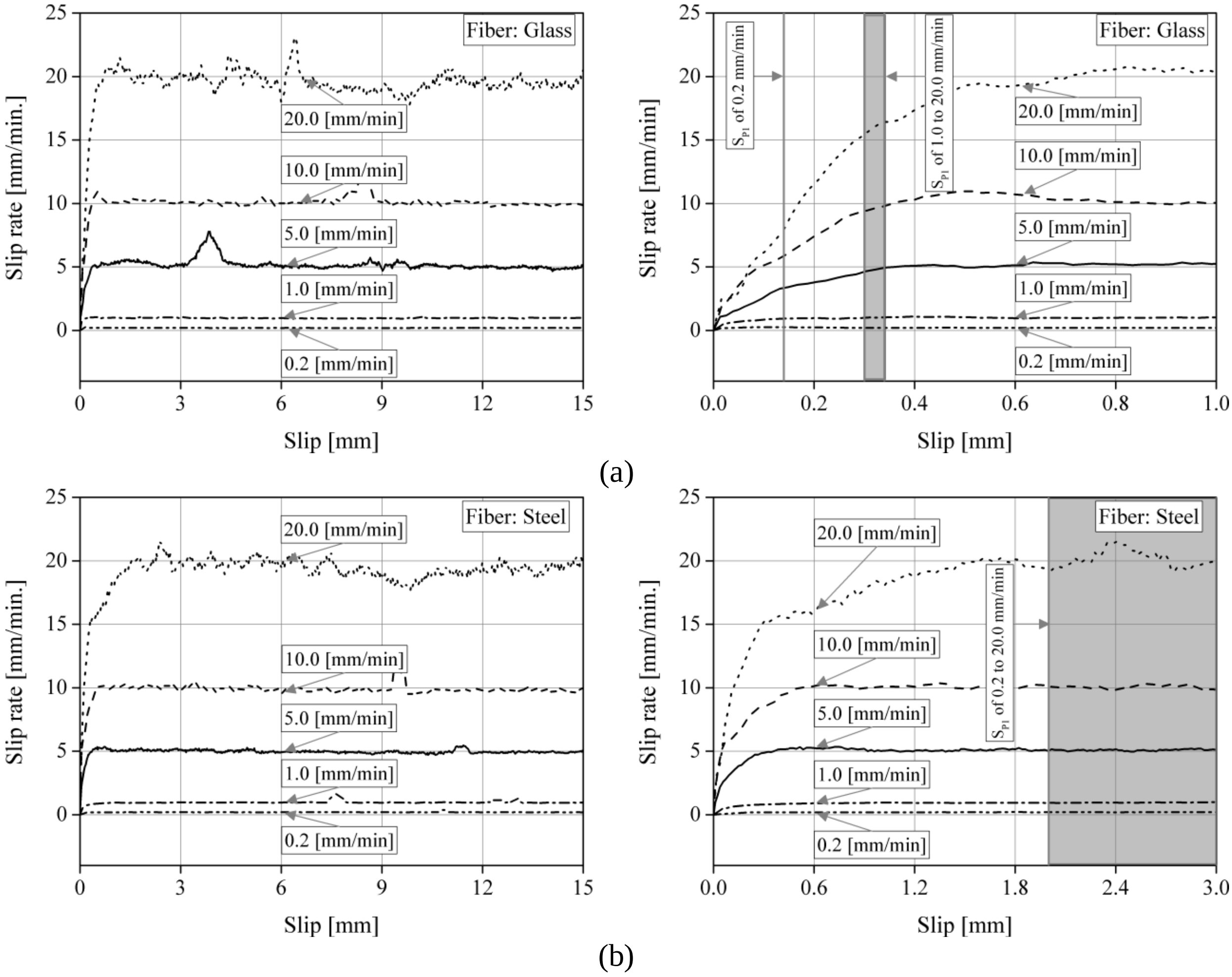

Fig. 2. Changes of slip rate vs. slip: (a) glass TRM; (b) steel TRM.

This paper can be found at https://doi.org/10.1617/s11527-021-01706-w

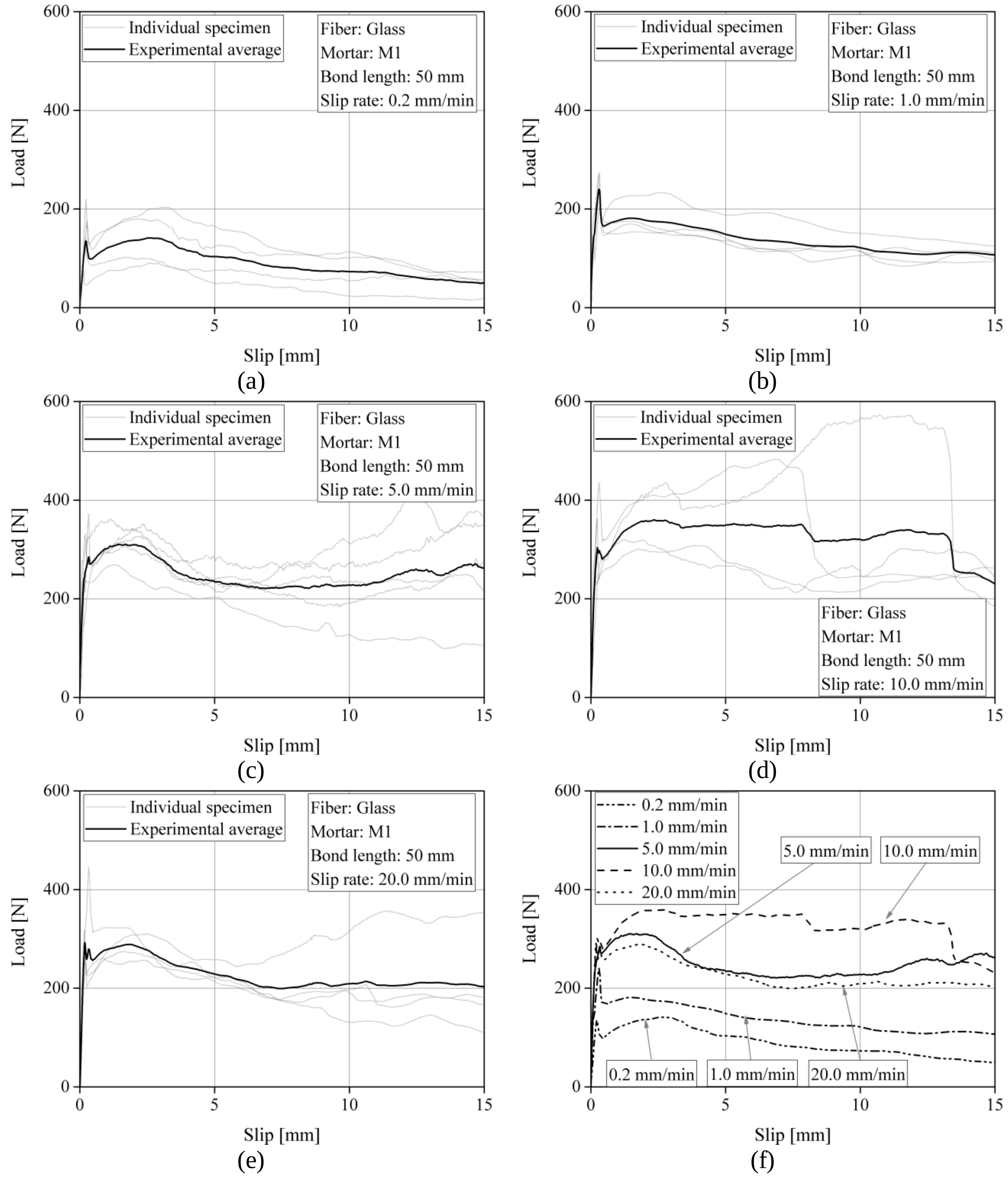

Fig. 3. Load-slip response curves of monotonic pull-out tests on glass TRM performed under different slip rates: (a) 0.2 mm/min; (b) 1.0 mm/min; (c) 5.0 mm/min; (d) 10.0 mm/min; (e) 20.0 mm/min; (f) average.

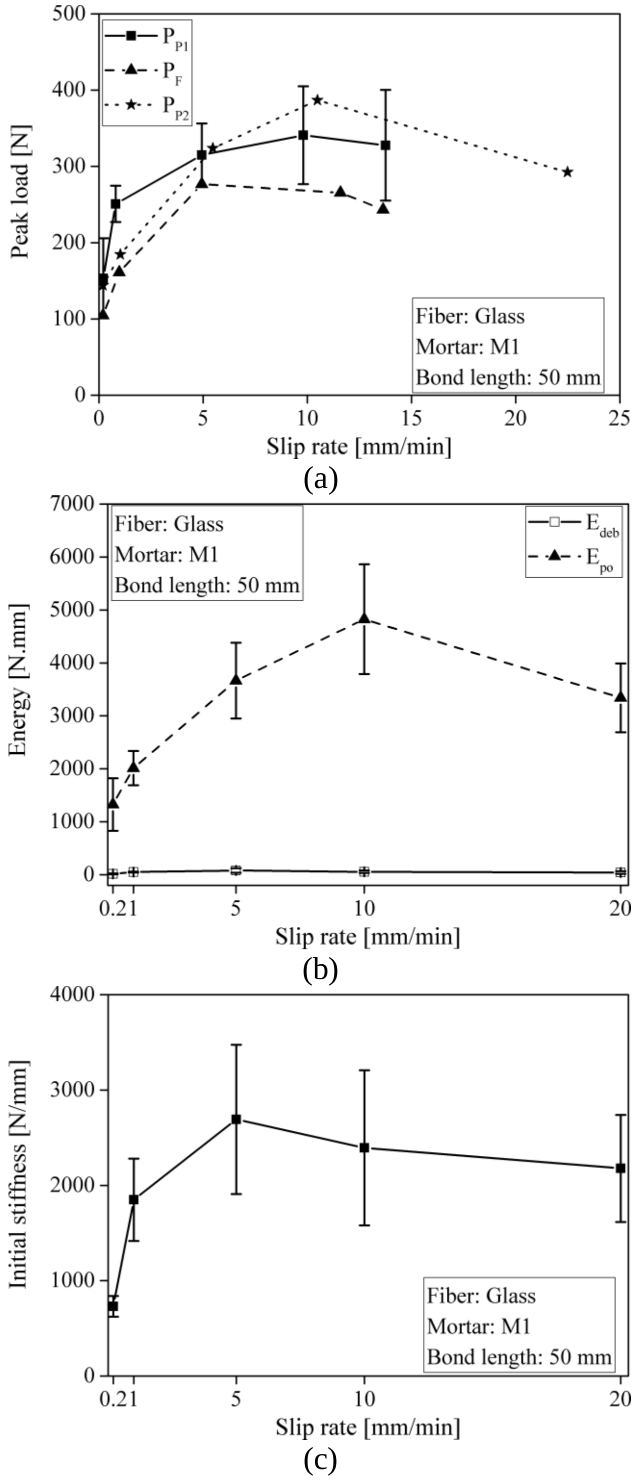

Fig. 4. Effect of the slip rate on the bond parameters of glass TRM in monotonic pull-out tests: (a) peak loads and frictional load; (b) pull-out and debonding energy; (c) initial stiffness.

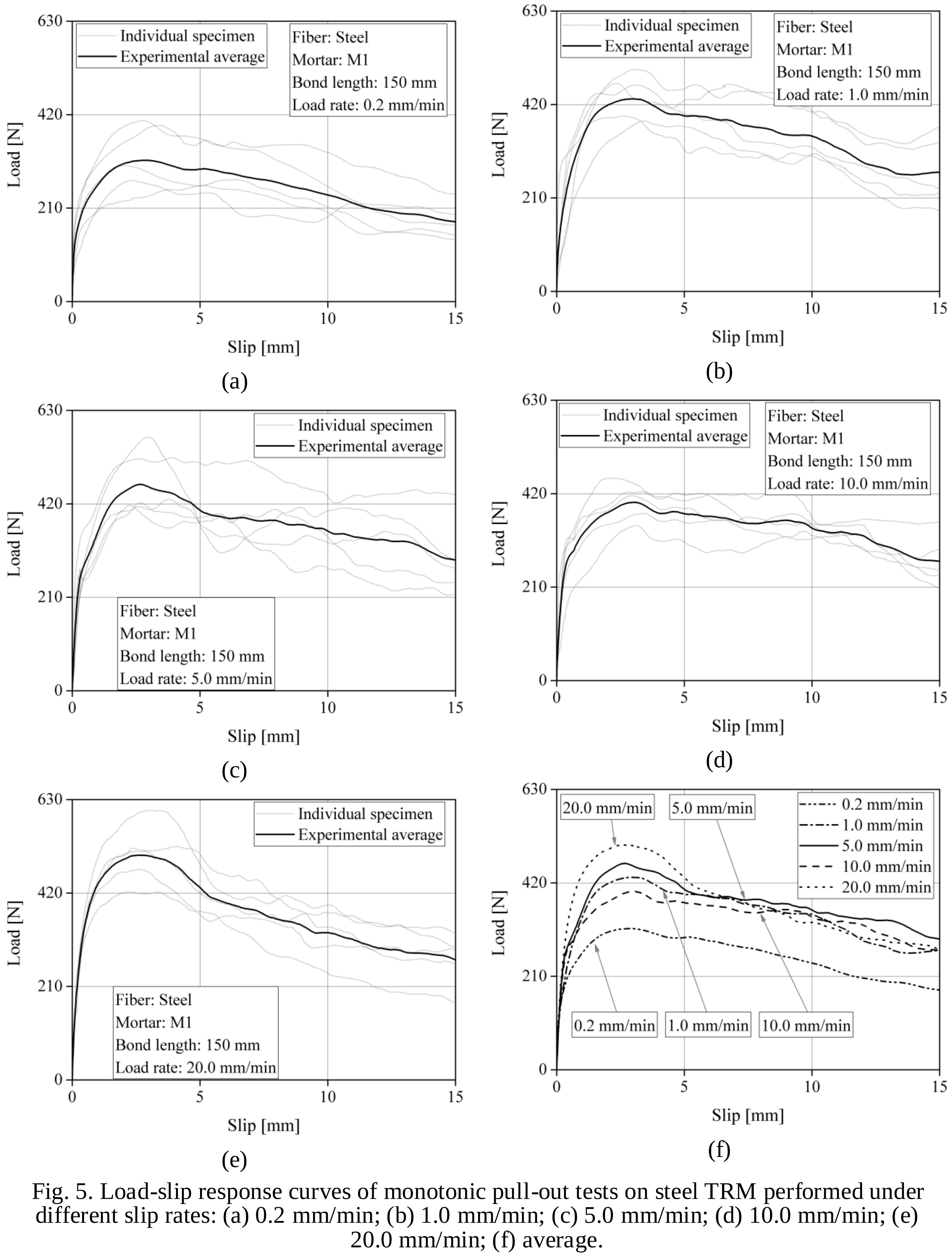

Fig. 5. Load-slip response curves of monotonic pull-out tests on steel TRM performed under different slip rates: (a) 0.2 mm/min; (b) 1.0 mm/min; (c) 5.0 mm/min; (d) 10.0 mm/min; (e) 20.0 mm/min; (f) average.

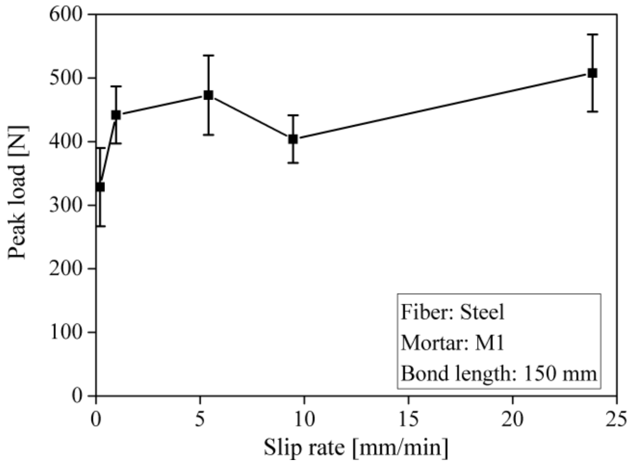

(a)

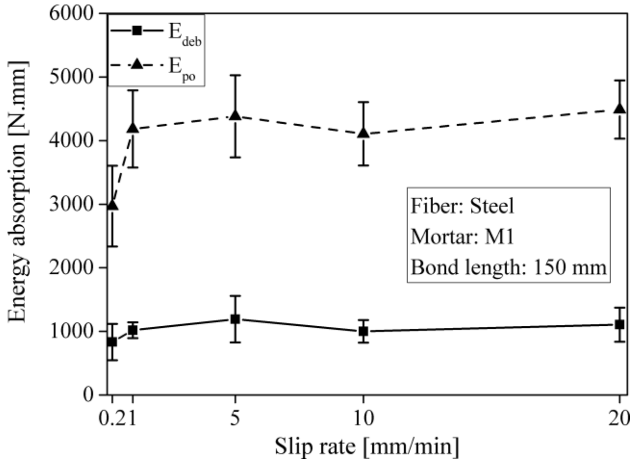

(b)

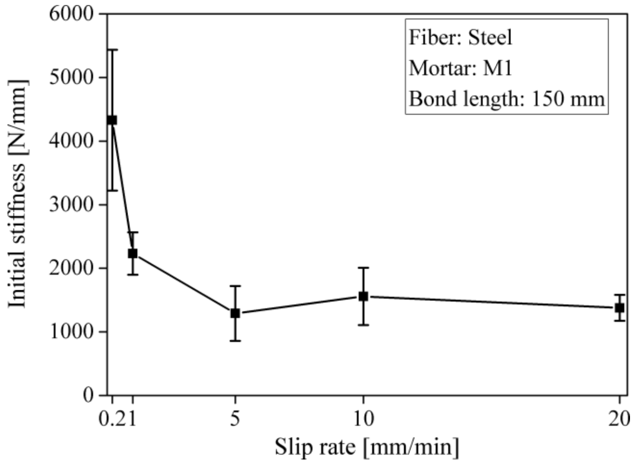

(c)

Fig. 6. Effect of the slip rate on bond parameters of steel TRM in monotonic pull-out tests: (a) peak loads; (b) pull-out and debonding energy; (c) initial stiffness.

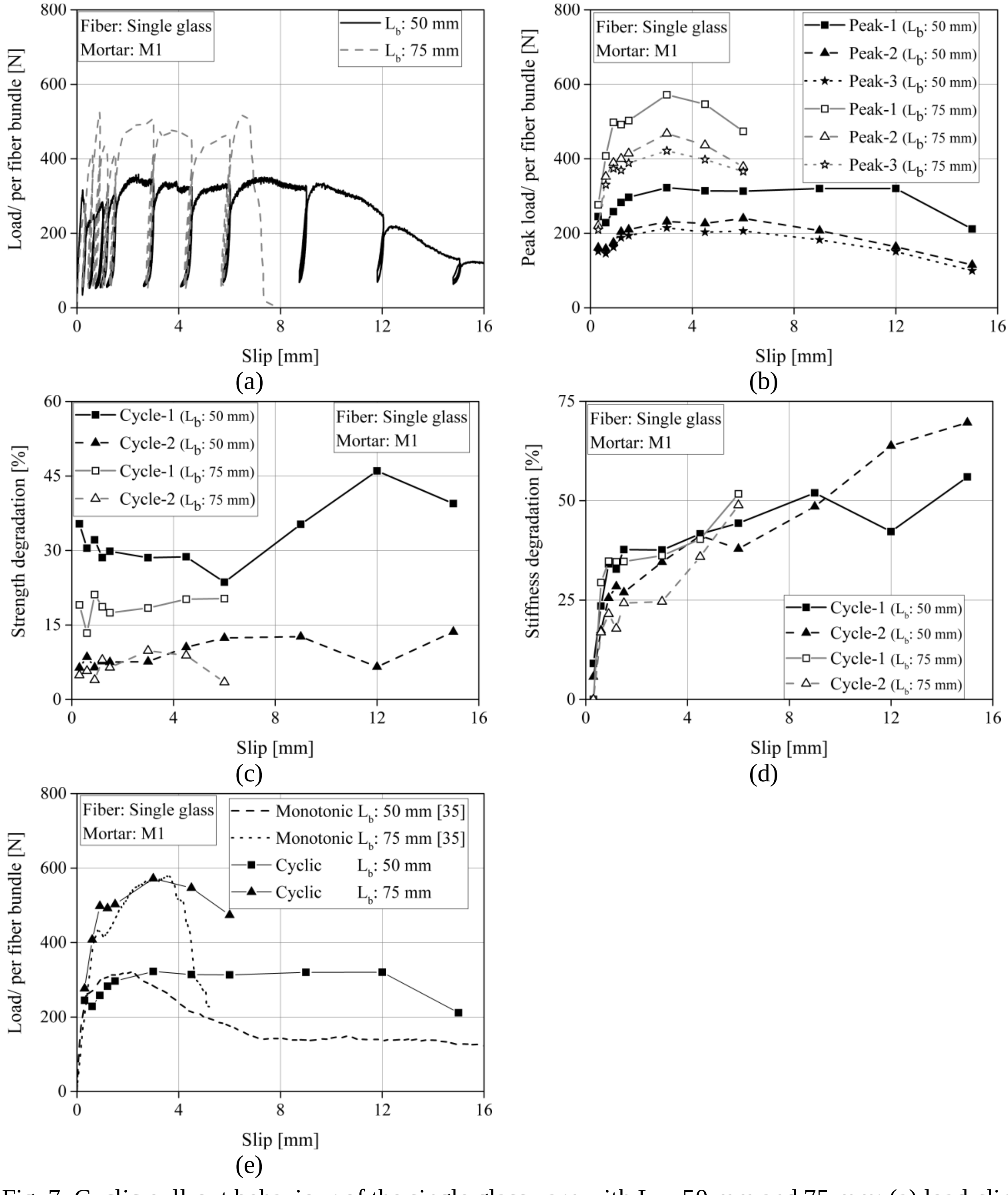

Fig. 7. Cyclic pull-out behaviour of the single glass yarn with L_b= 50 mm and 75 mm: (a) load-slip curve; (b) peak loads; (c) strength degradation; (d) stiffness degradation; (e) comparison of monotonic and push of cyclic loading (Peak 1).

This paper can be found at https://doi.org/10.1617/s11527-021-01706-w

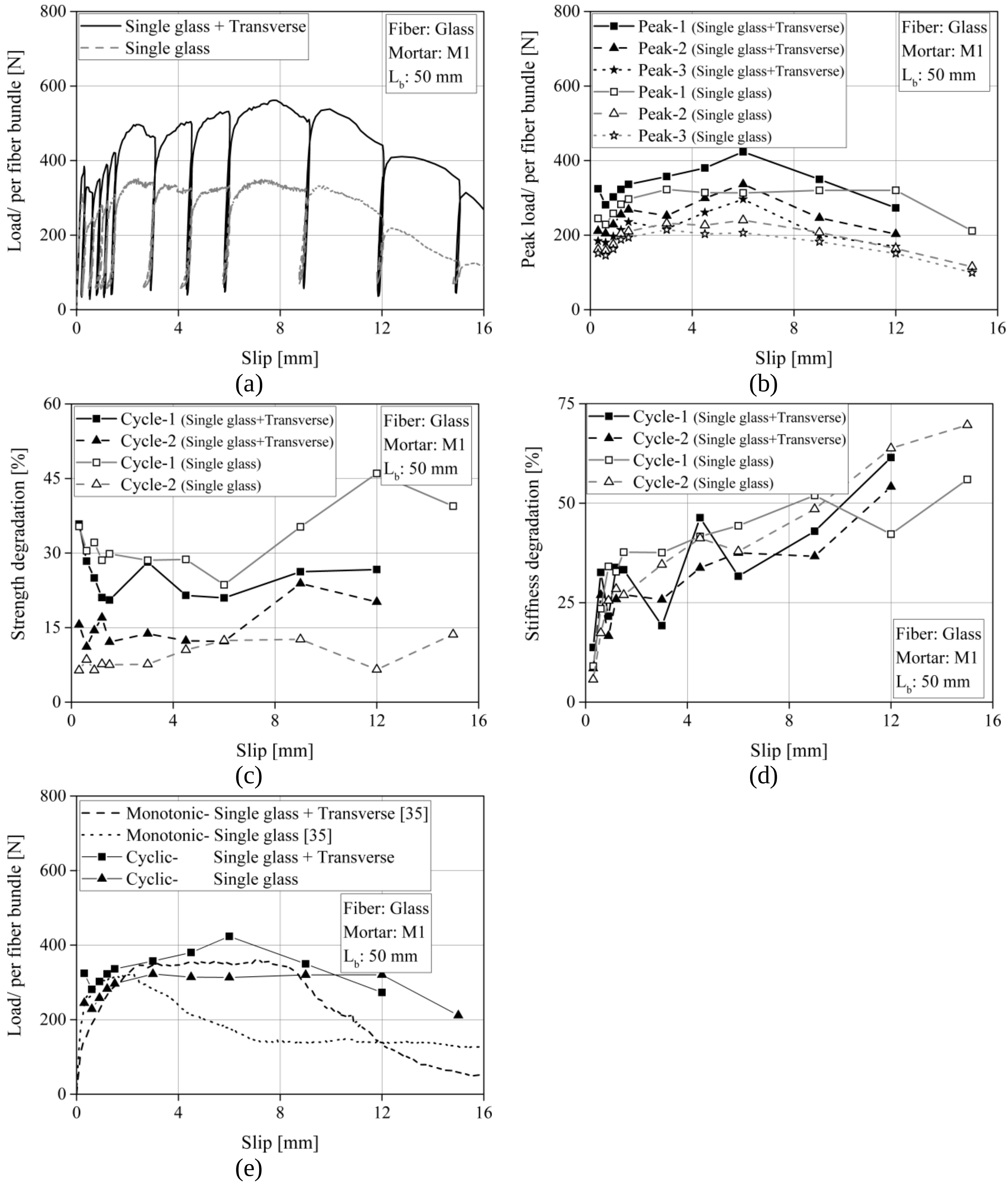

Fig. 8. Cyclic pull-out behaviour of the single glass yarn with and without transverse elements and L_b= 50 mm: (a) load-slip curve; (b) peak loads; (c) strength degradation; (d) stiffness degradation; (e) comparison among monotonic and cycling loading.

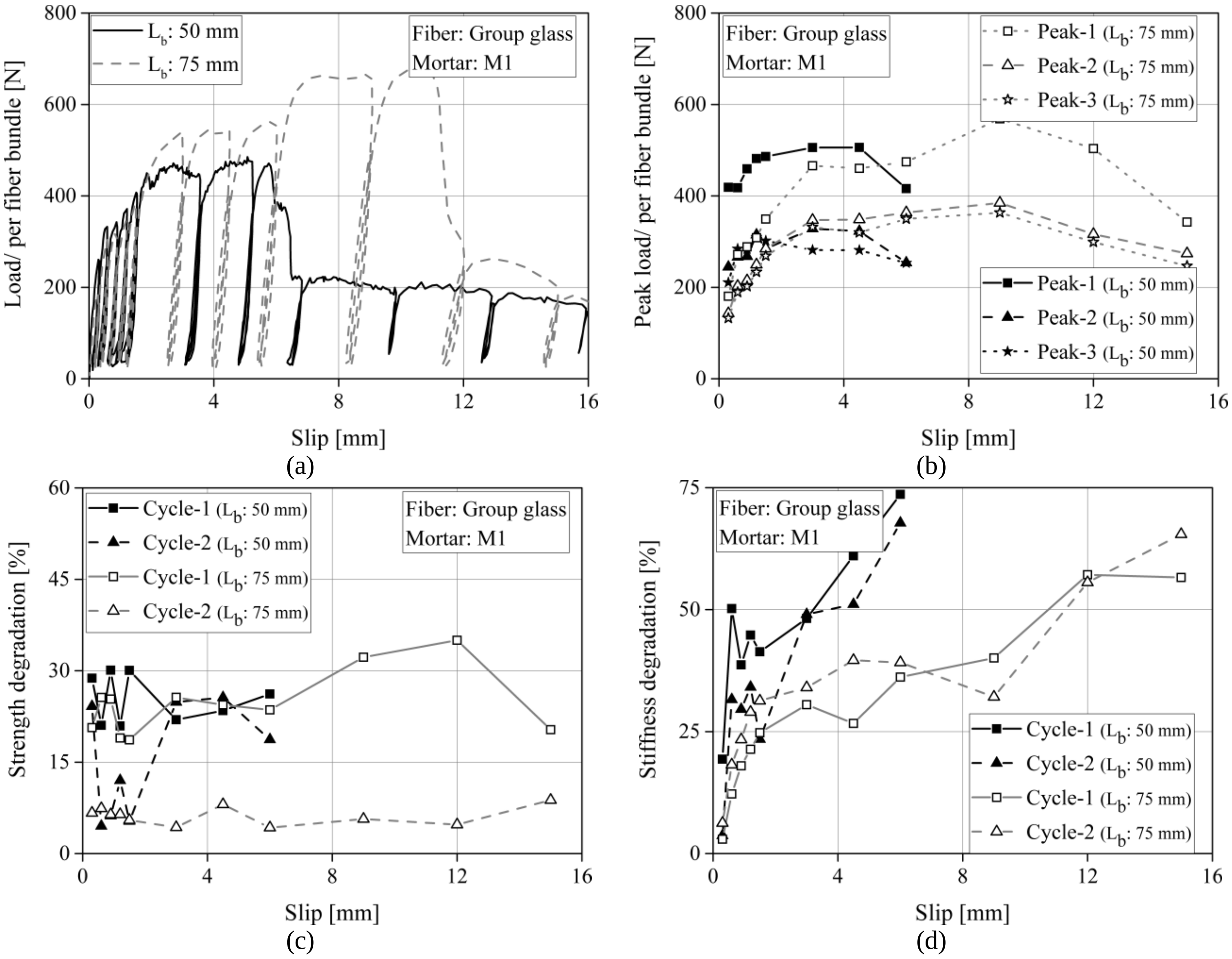

Fig. 9. Cyclic pull-out behaviour of the group of 2 glass yarns with L_b= 50 mm and 75 mm: (a) load-slip curve; (b) peak loads; (c) strength degradation; (d) stiffness degradation.

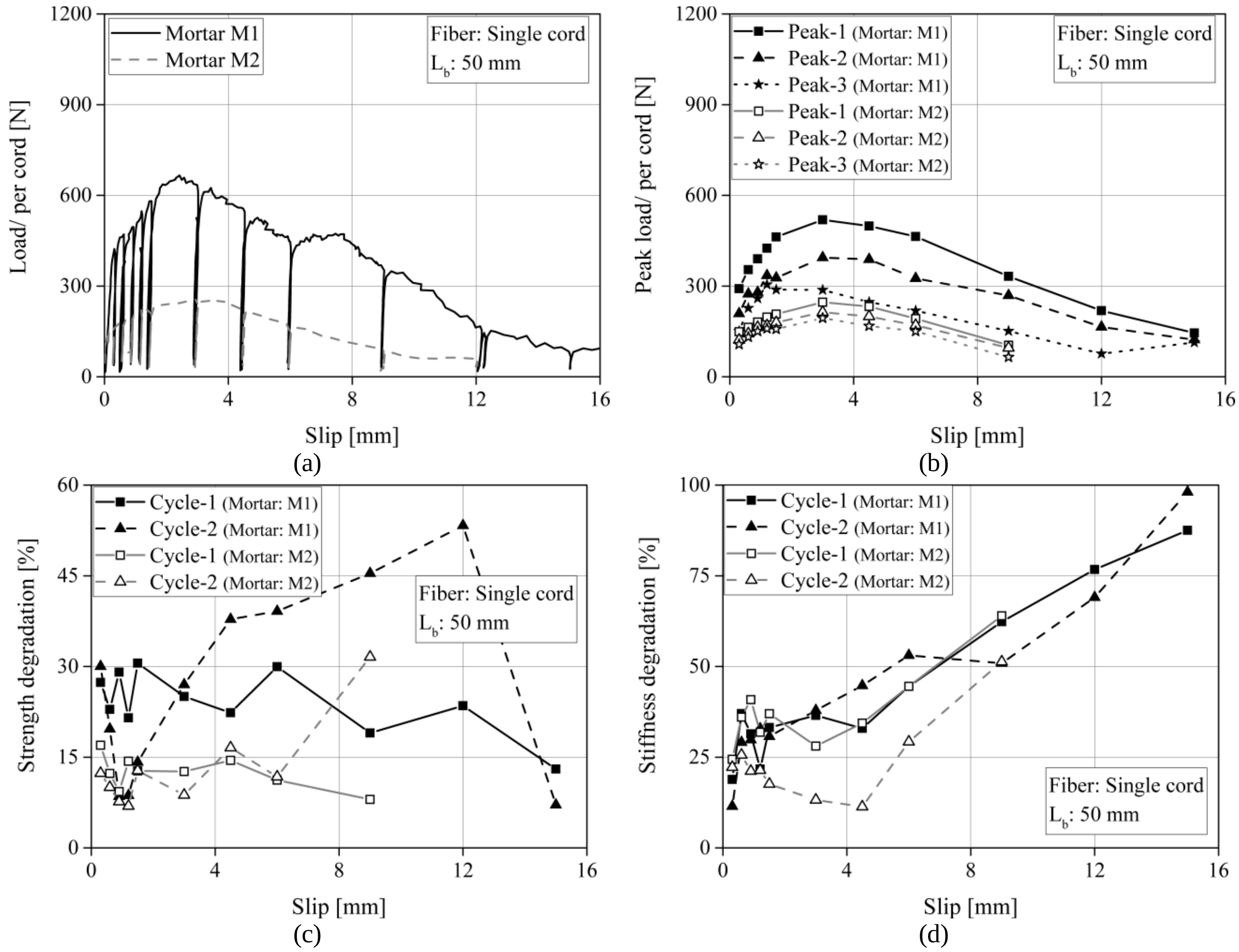

Fig. 10. Cyclic pull-out behaviour of the single UHTSS cord and mortars M1 and M2 with L_b=50 mm: (a) load-slip curve; (b) peak loads; (c) strength degradation; (d) stiffness degradation.

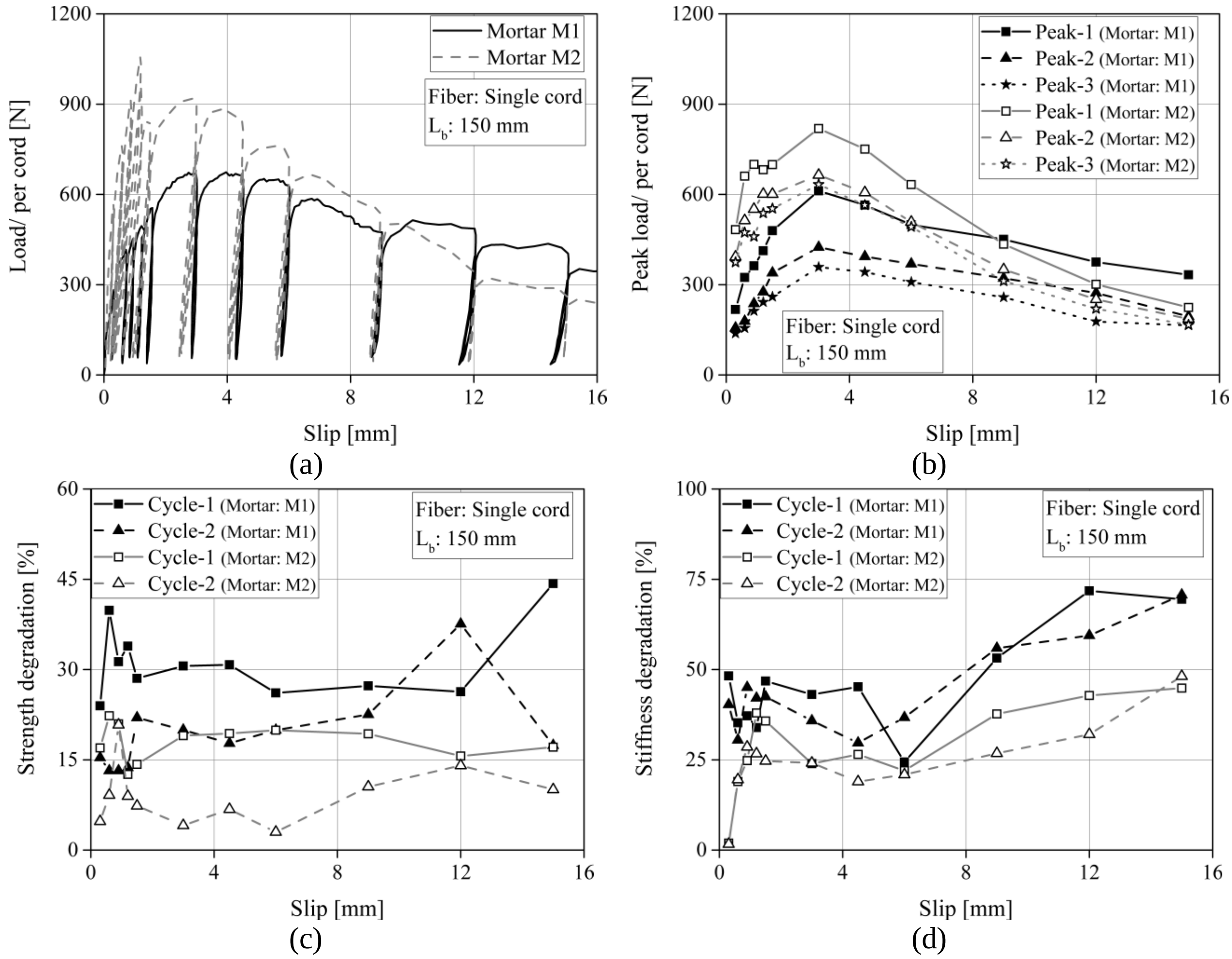

Fig. 11. Cyclic pull-out behaviour of the UHTSS cord and mortars M1 and M2 with L_b=150 mm: (a) an example load-slip curve; (b) peak loads; (c) strength degradation; (d) stiffness degradation.

This paper can be found at https://doi.org/10.1617/s11527-021-01706-w

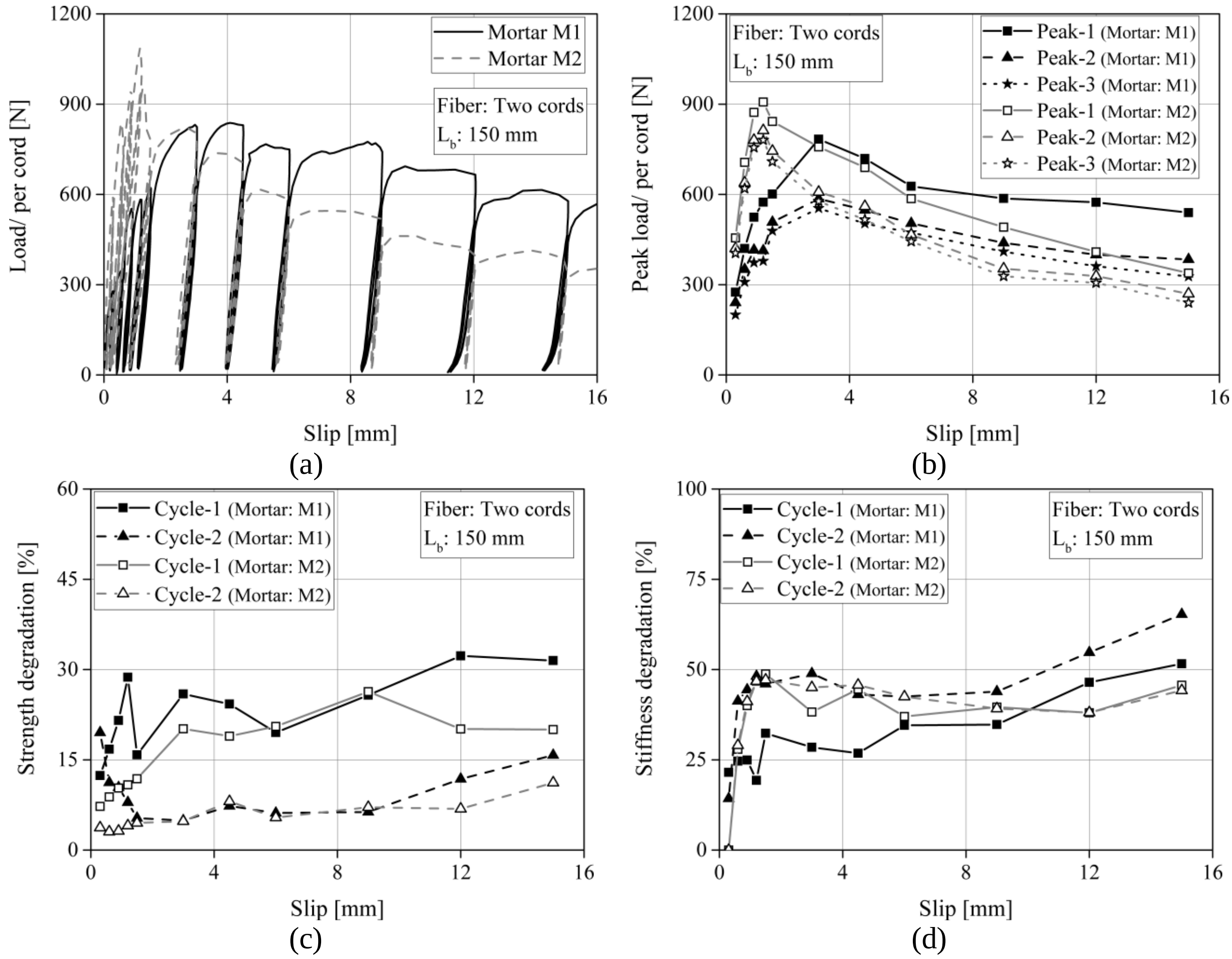

Fig. 12. Cyclic pull-out behaviour of the group of 2 UHTSS cords and mortars M1 and M2 with L_b=150 mm: (a) load-slip curve; (b) peak loads; (c) strength degradation; (d) stiffness degradation.

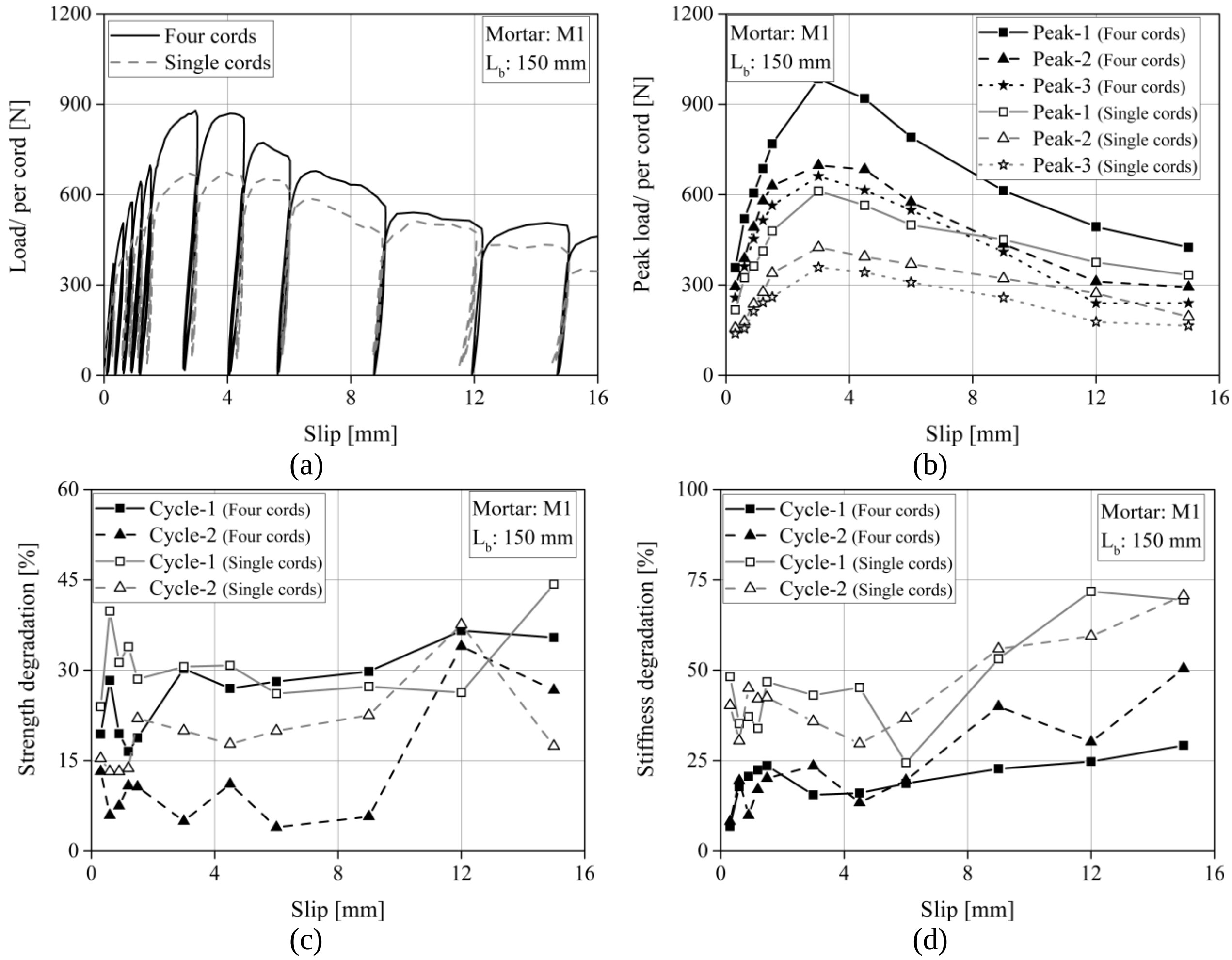

Fig. 13. Cyclic pull-out behaviour of the single cord and the group of 4 UHTSS cords and mortar M1 with L_b=150 mm: (a) load-slip curve; (b) peak loads; (c) strength degradation; (d) stiffness degradation.

Table 1. Pull-out experimental plan.

Type of test	Objective	Matrix	Textile	Textile configuration	L_b [mm]	Slip rate [mm/min]	Number of tests
Monotonic tests	Effect of slip rate on the textile-to-mortar bond behavior	M1	Glass	Single yarn	50	0.2	5
						1.0	5
						5.0	5
						10.0	5
						20.0	5
		M1	Steel	Single cord	150	0.2	5
						1.0	5
						5.0	5
						10.0	5
						20.0	5
Cyclic tests	Effect of cyclic loading on the textile-to- mortar bond behavior	M1	Glass	Single yarn	50	1.0 mm/min until 9 mm slip and 3.0 mm/min from 9 mm to the end of test	5
				Single yarn + transverse			5
				Group of 2 yarns			5
				Single yarn	75		5
				Group of 2 yarns			5
		M1	Steel	Single cord	50		5
					150		5
				Group of 2 cords	150		5
				Group of 4 cords			5
		M2		Single cord	50		5
					150		5
				Group of 2 cords	150		5

This paper can be found at https://doi.org/10.1617/s11527-021-01706-w

Table 2. Results of monotonic pull-out tests on glass and steel TRM: average values and CoV (%) in round brackets.

Textile	Slip rate [mm/min]	P_{P1} [N]	P_F [N]	P_{P2} [N]	E_{po} [N.mm]	G_d [J/mm^2]	E_{deb} [N.mm]	K [N/mm]	S_{P1} [mm]	S_F [mm]	S_{P2} [mm]
Glass	0.2	153.3 (34)	104.6 (41)	144 (34)	1327.1 (37)	0.008 (101)	17.1 (43)	730.9 (15)	0.21 (22)	0.31 (27)	2.38 (22)
	1.0	250.8 (9)	161 (8)	184.4 (16)	2012.7 (16)	0.022 (52)	51.5 (14)	1849 (23)	0.32 (7)	0.62 (29)	2.23 (37)
	5.0	314.8 (13)	276.8 (11)	323.9 (10)	3664.2 (20)	0.008 (141)	81.4 (54)	2692.4 (29)	0.37 (51)	0.5 (33)	1.72 (26)
	10.0	340.8 (19)	265.5 (13)	386.9 (19)	4825.3 (21)	0.021 (82)	56.1 (41)	2393.6 (34)	0.27 (30)	0.33 (27)	3.74 (54)
	20.0	327.7 (22)	243.4 (18)	292.3 (9)	3340.9 (19)	0.021 (71)	43.3 (60)	2177.9 (26)	0.22 (26)	0.35 (33)	1.52 (44)
Steel	0.2	328.5 (19)	-	-	2968.5 (21)	-	833.5 (34)	4327.9 (26)	3.13 (35)	-	-
	1.0	441.8 (10)	-	-	4182.8 (15)	-	1017.9 (12)	2230.7 (15)	2.92 (13)	-	-
	5.0	473.1 (13)	-	-	4381.9 (15)	-	1191.8 (31)	1290.2 (33)	3.1 (20)	-	-
	10.0	403.9 (9)	-	-	4106.1 (12)	-	1000.9 (18)	1557.7 (29)	3.03 (14)	-	-
	20.0	507.7 (12)	-	-	4487.6 (10)	-	1106.3 (24)	1378 (15)	2.6 (13)	-	-